Chapter 3

Ultralow-threshold ytterbium-doped glass laser fabricated by the solgel process

3.1 Introduction

Rare-earth ions (e.g., Er^{3+}, Nd^{3+}, Yb^{3+}, Ho^{3+}) are popular dopants for solid-state lasers due to their high efficiencies, long upper-level lifetimes, ability to generate short pulses, and straightforward incorporation into host materials including glasses and crystals [52]. In addition, the rare-earth aggregate emission spectrum spans many key wavelengths from 0.3 to 3 μm that are important for imaging, sensing, medical treatment, and communications. While rare-earth lasers have been built in large form factors for high-power laser cutting and defense applications, they can also be designed to be small, low power, and ultrasensitive to the environment. The laser resonator finesse, defined as the free spectral range (FSR) divided by the resonance linewidth, quantifies the loss and hence energy storage efficiency of a resonator. For a given cavity, higher finesse results in lower threshold for lasing. Lacovara measured a 71 mW threshold for a Yb^{3+}:YAG microchip laser with a cavity finesse of 57 [53]. Asseh demonstrated 230 μW threshold for a Yb^{3+}:SiO_2 fiber laser with a finesse of 630 [54]. Recently, the ultra high Q ($> 10^8$) toroid whispering-gallery resonator was invented [10]. The extremely low loss of this device enabled significant reduction of the threshold for an Er-doped silica solgel laser [20]. The Yb-doped silica toroid microcavity laser reported here has an on resonance finesse greater than 10,000.

The Yb-doped silica gain medium of this microlaser is fabricated on a silicon chip according to the solgel chemical synthesis method. The solgel technique for making thin films is attractive because it is low cost, fast, and extremely flexible [55]. Indeed, solgel techniques have been used to make optical couplers, Er^{3+}–Yb^{3+}-doped waveguide amplifiers, and even silica nanotubes [56, 57, 58]. A Yb^{3+},Al^{3+}:SiO_2 solgel fiber laser achieved a threshold of 80 mW launched power [59]. The author has developed a fiber-coupled Yb-doped silica solgel microtoroid laser with 1.8 μW threshold, which is believed to be the lowest threshold to date for any ytterbium-doped laser.

3.2 Solgel fabrication of silica thin-films

The laser's ytterbium-doped silica gain material is fabricated according to the well-known solgel technique. Solgel is a flexible and cost effective wet-chemistry synthesis method commonly utilized for preparation of glasses and ceramics. The applications of solgel materials are diverse, covering optics, electronics, chemistry, and biology. For instance, a novel field-effect transistor (FET) was recently reported with a zinc oxide (ZnO) thin film fabricated by the solgel technique [60]. The foundation for solgel fabrication was laid in the 1800s by Ebelman and Graham, who discovered that it was possible to synthesize silicon dioxide (silica) in gel form by hydrolysis of tetraethyl orthosilicate (TEOS) in an acidic environment [55]. This basic solgel technique, including TEOS and an acidic catalyst, survives today and forms the framework of the author's solgel fabrication of silica thin films for rare-earth doped microtoroid lasers. Research into practical applications for solgel fabricated glasses and ceramics exploded in the 1990s [55, 61]. A previous graduate student in the Vahala group, Lan Yang, developed solgel fabrication of erbium-doped silica thin films at Caltech. Lan demonstrated novel erbium-doped silica microsphere and microtoroid lasers [62, 63, 20].

Solgel fabrication of amorphous silica (SiO_2) can be divided into three main parts: hydrolysis to produce a colloidal suspension (sol), water condensation into a liquid phase gel, and high temperature annealing to form dense glass. Here, the general method of solgel fabrication of silica thin films will be discussed. Specific fabrication details will be given later in the chapter.

Simply put, the goal of solgel fabrication of silica is to create a dense and uniform network of silicon and oxygen atoms in a precise stoichiometric ratio ($\ldots - \mathrm{Si} - \mathrm{O} - \mathrm{Si} - \mathrm{O} - \ldots$). Of course, this silica network must be free of contaminants like water or $-$OH bonds, solvents, or organics in order for the final silica material to exhibit ultra-low loss in the infrared. A co-solvent, such as methanol or isopropanol, is included during the chemical reaction to allow thorough mixing of TEOS and water, which are normally immiscible.

3.2.1 Sol synthesis by hydrolysis

TEOS, with chemical formula $Si(OC_2H_5)_4$, is the metal alkoxide precursor for the solgel reaction. An alkoxide (represented as $-$OR) consists of an organic group (i.e., C_2H_5) bound to an oxygen atom, and is very reactive in the presence of proton donor molecules like water. The first fabrication step is hydrolysis, in which alkoxide groups ($-$OR) of TEOS are replaced by hydroxyl groups ($-$OH) as shown in Equation (3.1).

$$\mathrm{Si} - \mathrm{OR} \; + \; \mathrm{H} - \mathrm{O} - \mathrm{H} \longrightarrow \mathrm{Si} - \mathrm{OH} \; + \; \mathrm{R} - \mathrm{OH} \tag{3.1}$$

The acidic catalyst (HCl) for the hydrolysis reaction adds protons (H^+) to the alkoxide groups, and makes them more reactive with water. The mixture of alkoxide gel precursors (Si$-$OH molecules)

is named the colloidal solution (sol).

3.2.2 Gel synthesis by condensation

Next, the alkoxide gel precursors undergo a polymerization reaction with the acid catalyst. This reaction produces cross-linked polymer chains of silicon and oxygen, which are the foundation of the silica network, and also causes water condensation as shown in Equation (3.2). Two hydrolyzed Si-OH molecules are linked together in the condensation reaction to form a siloxane (Si−O−Si) bond.

$$\mathrm{Si-OH + Si-OH \longrightarrow -Si-O-Si- + H-OH} \tag{3.2}$$

During condensation, the sol particles form a continuous liquid phase (gel) of silicon and oxygen chains surrounded by water, organics, and co-solvent. Moderate heating, at less than 100°C to prevent evaporation of water, is commonly used to speed up the hydrolysis and condensation reactions.

The next important step for solgel fabrication is drying. Water and solvent are removed from the interconnected pores of the gel, and the polymer chain aggregation increases as the gel is dried at room temperature. If the solvent and water cannot evaporate easily, microcracks form as non-uniform gel shrinkage builds up stress. Cracking is normally found only in larger solgel bulk material (1 mm or larger) and can be eliminated through careful control of the solgel chemistry.

3.2.3 Glass densification by heat treatment

The dry gel with silica pores is then subjected to a high temperature heat treatment in the final solgel fabrication step, normally at 1,000°C or higher for silica. During high temperature annealing, any remaining organics are forced out of the silica gel, additional polycondensation occurs, the pores disappear, and the silica network is densified. After the heat treatment is complete, the density of a well fabricated solgel silica glass is equal to fused silica. Yang measured the Fourier Transform Infrared (FTIR) spectrum of a silica solgel thin film after high temperature annealing, and showed that it closely matches the spectrum of wet-deposition thermal oxide [20]. Another method for verifying the quality of silica is by measuring the buffered-oxide etching (BOE) speed. The author measured that the ytterbium-doped silica solgel thin film (1.5 μm thick) has an etch rate of 13 Å/s, identical to fused silica, which confirms the correct density of solgel silica.

3.3 Ytterbium activated silica for laser gain

If properly excited by pump radiation, ytterbium ions can provide laser gain by stimulated emission in host materials like silicate glass or yttrium aluminum garnate (YAG) crystal. For solgel fabrication of glass thin films, silica can be doped with ytterbium by adding ytterbium nitrate, $Yb(NO_3)_3$, to the initial solution. In this way, silica can be doped with virtually any rare-earth ion, showing the great flexibility of solgel fabrication.

The first ytterbium-doped silica laser on record was demonstrated in 1962 by Etzel [64]. The ytterbium laser cavity can be a fiber, microchip, or microtoroid like the laser presented here [53, 54, 19].

3.3.1 Electronic structure of ytterbium

One of the most attractive features of ytterbium for laser action is its simple electronic structure, consisting of only the ground manifold ($F^2_{7/2}$) and excited manifold ($F^2_{5/2}$) [65]. As shown in Figure 3.1, the ground manifold has four Stark levels and the excited manifold has three Stark levels. The Stark levels are formed by splitting of the spectral lines of the ytterbium atoms by the silica network's electric field.

The large energy gap between the ground and excited manifolds prevents non-radiative decay, increasing the laser's upper-level lifetime (τ_{Yb}). Also, no laser up-conversion is expected for ytterbium silica due to the lack of higher electronic states [65]. Erbium doping cannot exceed 1%, or else deleterious concentration-quenching will reduce the laser efficiency. Ytterbium does not suffer from this effect and can be doped to much higher concentrations, even exceeding 20%.

3.3.2 Ytterbium laser characteristics

Ytterbium has a broad absorption line centered on 920 nm, and a narrow absorption peak near 970 nm with higher cross section of absorption. All of the ytterbium lasers discussed in this thesis are optically pumped on the 970 nm line, which has a 10 nm full-width at half-maximum (FWHM) absorption peak. Ytterbium can have higher pump efficiency than erbium because ytterbium's cross section of absorption ($\sigma_{a,Yb}(975\text{nm}) = 2.5 \times 10^{-24}\text{m}^2$) is larger than erbium ($\sigma_{a,Er}(1460\text{nm}) = 2 \times 10^{-25}\text{m}^2$). Figure 3.2 is a plot of the cross sections of absorption and emission versus wavelength for $Yb{:}SiO_2$. Ytterbium has a large emission cross section from $1010-1050$ nm, with emission being observed even as high as 1200 nm. Ytterbium-doped tunable lasers take advantage of this large emission bandwidth [66].

In this thesis, the ytterbium-doped silica lasers are pumped at 970 nm and laser emission is generated around 1040 nm. The small quantum defect, $(\lambda_{laser} - \lambda_{pump})/\lambda_{pump} = 7\,\%$, is an important advantage for ytterbium because the laser cavity generates significantly less heat than a correspond-

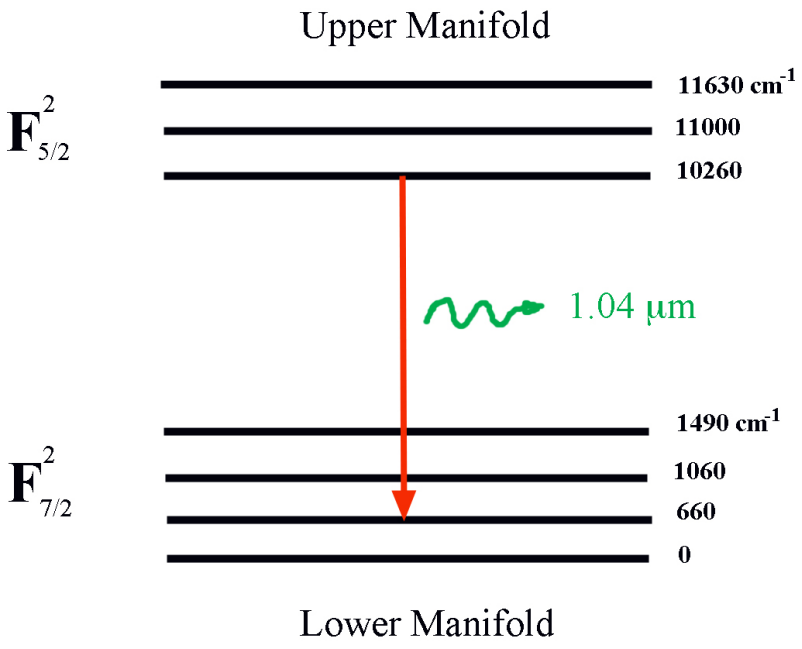

Figure 3.1. Energy level diagram for Yb^{3+}, showing the ground manifold ($F^2_{7/2}$, four Stark levels) and excited manifold ($F^2_{5/2}$, three Stark levels). The energy in wavenumbers (cm^{-1}) of each level is shown. Also, one of the primary laser transitions ($\lambda = 1.04\,\mu m$) is marked with a red arrow.

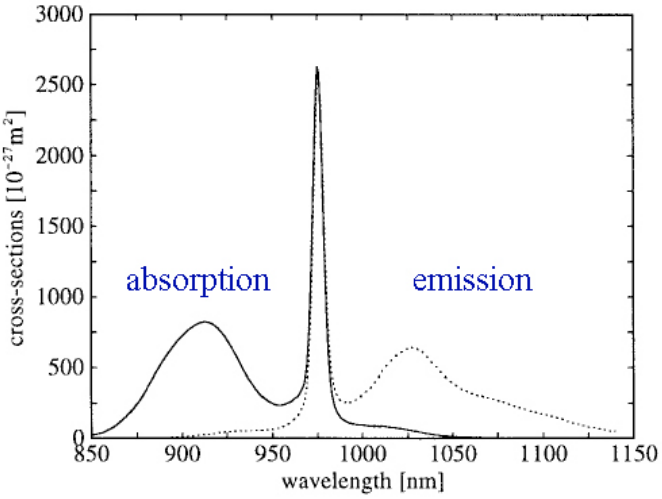

Figure 3.2. Absorption and emission cross-sections of $Yb^{3+} : SiO_2$ reproduced from Paschotta et al. [67]. The microtoroid lasers are pumped at 970 nm, laser emission is normally at 1040 nm.

ing neodymium-doped laser. Low laser heating is important for high power lasers [68] and will also be beneficial for laser cooling applications. Ytterbium's pump and emission wavelengths are similar, allowing efficient fiber taper coupling of the pump and laser radiation using a single fiber taper.

To summarize, ytterbium is an attractive laser dopant because of its high cross section of absorption, low quantum defect, simple electronic structure, and high concentration doping capability. In addition, the 1 μm emission wavelength of ytterbium is very useful, as will be discussed in **Chapter 4**.

3.4 Yb:SiO_2 laser modeling

3.4.1 Laser model parameters

A laser model of the Yb:SiO_2 microtoroid was developed to determine the design parameters of the laser and anchor the experimental results. The author modified a microtoroid laser model, developed for erbium silica microlasers by Min [21], for the ytterbium silica microtoroid laser resonator. This model is based on a coupled-mode theory of a microtoroid resonator and fiber taper waveguide [69, 70, 13, 71].

Several constants must be included to properly model the laser dynamics. The cavity mode volume, V, is calculated as $V = (2\pi R_{toroid})(\pi r_{mode}^2)$. The coupling factor ($\kappa_{ext} = \sqrt{1/\tau_{ext}}$) is the amplitude coupling coefficient between the toroid and the taper's pump wave. The extrinsic microtoroid cavity lifetime ($\tau_{ext} = Q_{ext}/2\pi f_s$) is influenced by the coupling between the taper and toroid, in addition to intrinsic cavity loss factors. Next, define several parameters that model the gain properties of the laser (also known as Giles parameters).

$$\begin{aligned} \alpha_p &= \Gamma N_T \sigma_p^a \ , \ \alpha_s = \Gamma N_T \sigma_s^a \\ g_p^* &= \Gamma N_T \sigma_p^e \ , \ g_s^* = \Gamma N_T \sigma_s^e \end{aligned} \tag{3.3}$$

The overlap factor, Γ, represents the physical overlap of the cavity pump and signal modes inside the microtoroid. The near ideal phase matching between the microtoroid mode and taper mode, and the small cavity mode volume are expected to give an overlap factor approaching unity. The similar pump and signal wavelengths ($\lambda_p = 970$ nm, $\lambda_s = 1040$ nm) of ytterbium also contribute to the large overlap factor. Therefore, $\Gamma = 1$ will be assumed for the ytterbium laser modeling. The ytterbium concentration, N_T, has been modeled within the range of 2×10^{18} to 1×10^{20}. Ytterbium's pump and signal absorption and emission are given by σ, whose values can be found in literature [67]. The cross section values used for simulations in this research are given in Table 3.1.

$\sigma_p^a = 2.7 \times 10^{-24}$ m^2	$\sigma_s^a = 1.0 \times 10^{-26}$ m^2
$\sigma_p^e = 2.7 \times 10^{-24}$ m^2	$\sigma_s^e = 5.0 \times 10^{-25}$ m^2

Table 3.1. Pump and signal cross sections of absorption and emission for Yb:SiO_2

Also, passive cavity loss terms are defined at both pump and signal wavelengths as

$$\alpha_{p,passive} = 2\pi \frac{n_p}{\lambda_p Q_{passive}} \ , \ \alpha_{s,passive} = 2\pi \frac{n_s}{\lambda_s Q_{passive}} \tag{3.4}$$

where $Q_{passive}$ is the loaded quality factor ignoring the absorption due to ytterbium ions. The room-temperature refractive indices of silica at the pump and signal wavelengths are given by n_p and n_s. The long laser upper-level lifetime of ytterbium silica ($\tau_{Yb} = 0.7$ ms), while not as large as erbium's (10 ms), enables high laser efficiency as already demonstrated in a fiber laser [72]. To account for the absorption by ytterbium ions, an appropriate absorption coefficient is defined as $\alpha_{yb} = \frac{n_s}{c\tau_{yb}}$.

3.4.2 Laser pump threshold

After applying coupled-mode theory to the microtoroid and taper system, the ytterbium microtoroid laser's threshold power for laser operation can be derived [21].

$$\begin{aligned} P_{th} =& N_t h\nu V \left(\frac{f_s n_s}{f_p n_p}\right)\left(\frac{c^2}{4n_p^2\kappa_p^2}\right) \\ &\times \frac{\left[(\alpha_p + \alpha_p^{passive})(\alpha_s + g_s^*) - (\alpha_p + g_p^*)(\alpha_s + \alpha_s^{passive})\right]^2}{(\alpha_s + g_s^*)^2} \\ &\times \frac{\alpha_{Yb}(\alpha_s + \alpha_s^{passive})}{\alpha_p(\alpha_s + g_s^*) - (\alpha_p + g_p^*)(\alpha_s + \alpha_s^{passive})} \end{aligned} \tag{3.5}$$

P_{th} is the absorbed pump power at which the round-trip laser gain is equal to the round-trip loss, and pump powers above threshold will generate laser emission. In addition to threshold, the laser output power and efficiency can be easily calculated [21]. Microtoroid lasers doped with erbium or ytterbium normally have threshold pump powers on order of 10 μW, record values for rare-earth doped lasers. Low thresholds are made possible by small cavity diameters, low doping levels (of order 0.1% or less) and efficient taper fiber coupling.

3.4.3 Laser model results

The author used the laser model described above to determine an optimum doping concentration and toroid diameter for laser experiments. The ytterbium concentration was adjusted to minimize

the pump threshold, and made possible development of a record-low threshold ytterbium laser. The laser threshold dependence on doping concentration is shown in Figure 3.3. The lower panel highlights the low concentration behavior, which shows a rapid increase in pump threshold as the concentration is reduced. Lasing is not predicted for ytterbium concentrations less than 2.9×10^{18} cm^{-3}. There is a local minimum for laser threshold at $N_T = 3 \times 10^{18}$ cm^{-3}, around which the threshold increases. At lower concentrations, the threshold increases because the ytterbium ions must be pumped at a higher rate to overcome the intrinsic loss of the cavity and taper system. For concentrations higher than the optimum, the threshold increases since the additional ions must be pumped to transparency. Ytterbium is a quasi-three level laser, meaning it has ground state absorption due to room-temperature occupation of the lowest energy level.

As part of the ytterbium laser design exercise, the threshold dependence on major diameter was modeled. Figure 3.4 shows the linear relationship between laser threshold and toroid diameter for a ytterbium doping concentration of $N_T = 8 \times 10^{18}$ cm^{-3}. Smaller mode volume requires less pump power to reach the gain necessary for laser output. Based on the results of threshold simulations for dependence on toroid size and doping concentration, a suitable solgel fabrication produced microtoroids with record low threshold. For that laser, to be discussed in later sections, the toroid diameter (D) is 43 μm, and the doping concentration (N_T) is 4×10^{18} cm^{-3}.

The dependence of quality factor on ytterbium concentration shows the influence of the laser ions on cavity loss. At the pump wavelength (near 970 nm), the Q of the ytterbium doped microtoroid cavity is low due to the necessary pump absorption. Far away from the ytterbium absorption lines, at 1550 nm for example, the cavity Q is as high as the Q of undoped solgel silica microtoroids ($Q = 2.5 \times 10^7$), indicating that the scattering loss of the ytterbium ions is negligible. The on-resonance Q depends inversely on the doping concentration as shown in Figure 3.5. In this figure, both the model predictions shown in red, and the actual experimental Q agree well. As expected, higher Yb concentration gives lower Q due to the useful laser ion absorption.

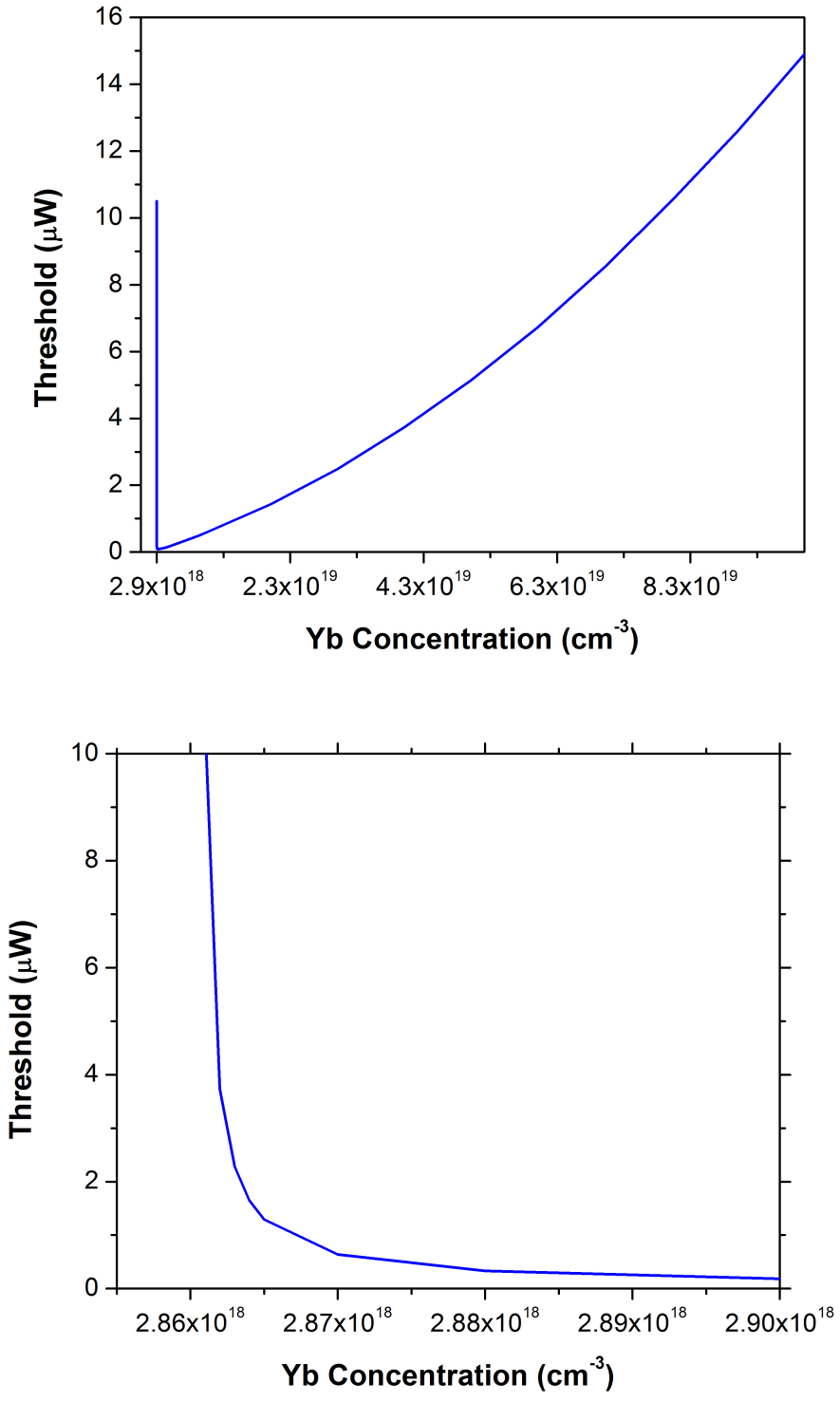

Figure 3.3. Plot of model predictions of Yb:SiO_2 laser threshold as a function of ytterbium concentration (N_T) for a $D = 43$ μm microtoroid. The lower panel shows more detail at low concentrations, where the laser threshold increases rapidly.

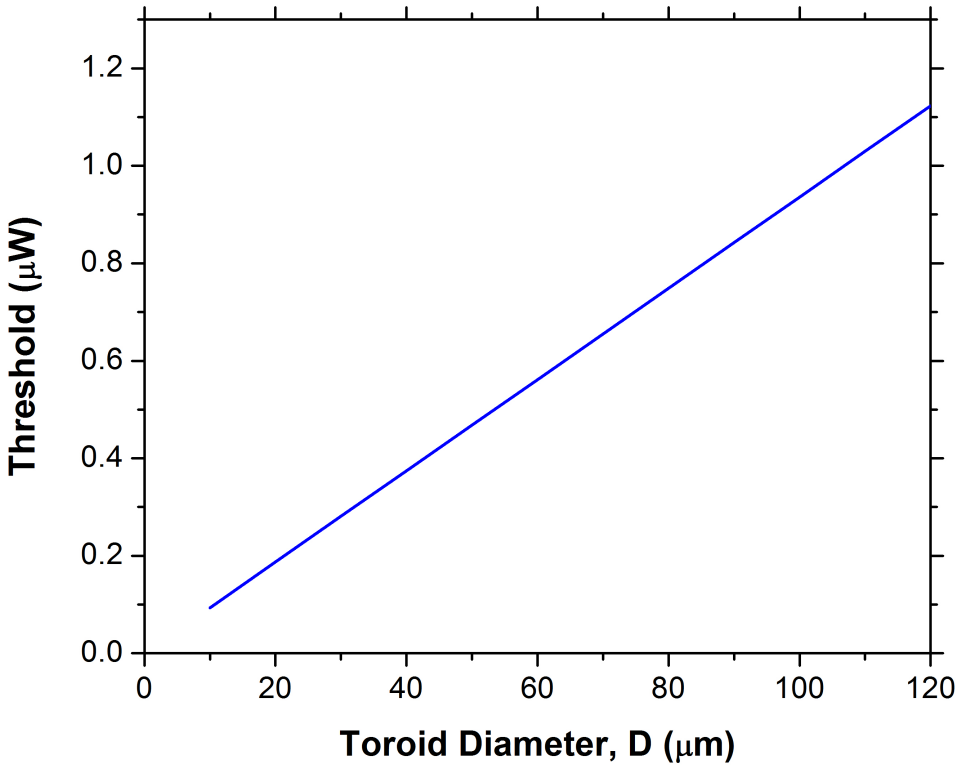

Figure 3.4. Plot of Yb:SiO_2 laser threshold as a function of toroid major diameter (D) for $N_T = 1 \times 10^{19}$ cm^{-3}

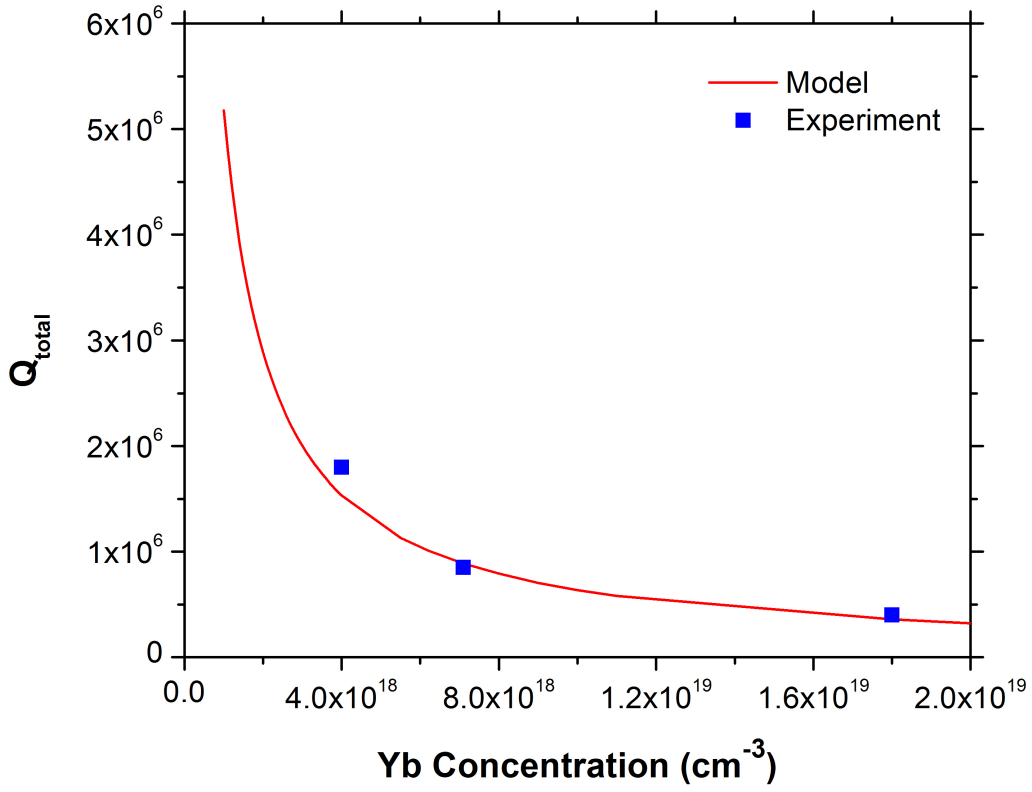

Figure 3.5. Yb:SiO_2 laser Q at the pump resonance as a function of the Yb concentration – the model prediction (red line) and experimental results (blue points) agree well. The Q decreases with Yb concentration as expected.

3.5 Yb:SiO_2 laser fabrication

3.5.1 Silica thin film preparation by the solgel method

Fabrication of the laser microcavity begins with solgel synthesis of the Yb-doped silica thin film, and closely follows the general solgel fabrication given in Section 3.2. First, tetraethoxysilane (TEOS) is hydrolyzed with a molar ratio of water to TEOS between 1:1 and 2:1. Isopropanol is the co-solvent and hydrochloric acid the catalyst. After the alkoxide groups in TEOS are replaced with hydroxyl groups, the remaining hydrogen atoms are removed through a condensation reaction. Finally, Yb nitrate is introduced to produce the desired Yb^{3+} concentration in the silica thin film. The entire mixture is stirred on a hot plate at 70°C for 3 h to produce the solgel liquid. The general solgel recipe including the quantity of each specific chemical is given in Table 3.2. While this recipe will produce undoped silica, rare-earth ions, like Yb^{3+} in the form of ytterbium nitrate, can be added. Since ytterbium nitrate is normally dissolved in water, the solgel engineer must adjust the added water so the total water mass is 1.4 g. After the heat-assisted chemical reaction, the Yb-doped silica solgel is deposited in three layers onto a silicon substrate by spin coating. Immediately after each layer is deposited, the thin film is annealed at 1,000°C in normal atmosphere for 3 h to remove the solvent, undesired organics, and hydroxyl groups in the solgel network [73, 74]. During solgel fabrication, only fresh chemicals (especially TEOS) clean glassware should be used in order to produce a high-quality silica solgel free of cracking.

Chemical Name	**Formula**	**Mass (g)**
Water	H_2O	1.40
Isopropyl Alcohol	C_3H_7OH	11.00
Hydrochloric Acid	HCl	1.10
Tetraethylorthosilicate	$SiC_8H_{20}O_4$	12.45

Table 3.2. solgel recipe for pure silica. Dopants like ytterbium nitrate can be included, and any water added for dilution should be included in the total water mass.

3.5.2 Microtoroid fabrication

After the solgel silica thin film is complete, the glass film is patterned by standard lithography and isolated silica disks are defined on the silicon substrate using a buffered oxide wet etch. The disks are then optically isolated from the underlying silicon using XeF_2 to selectively etch silicon, leaving Yb^{3+}:SiO_2 disks supported by silicon pillars. In the final step, a CO_2 laser (10.6 μm) symmetrically reflows the silica microdisk to form a smooth microtoroid with a 40 μm principal diameter. Surface tension during melting defines the toroid shape and increases the cavity quality factor by significantly

reducing surface roughness.

3.6 Laser testing

3.6.1 Experimental setup

A single submicrometer diameter fiber taper, which is phase matched to the microcavity's whispering gallery spatial mode, couples light into and out of the microtoroid at the equatorial plane as shown in Figure 3.6 [13, 8]. The coupling parameter, which determines the cavity loading and consequently the laser performance, is precisely adjusted by moving the silica cavity with respect to the fiber taper using a three-axis nano-positioning system.

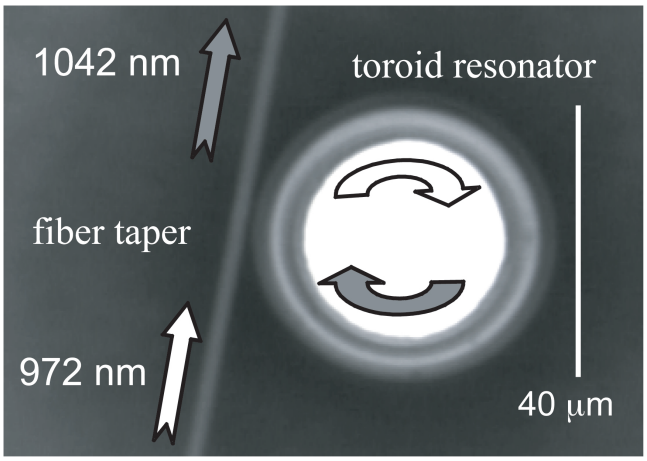

Figure 3.6. Top-view photograph of testing setup showing evanescent coupling of fiber taper to Yb^{3+}:SiO_2 microtoroid laser

A tunable, single-frequency, narrow linewidth 300 kHz semiconductor diode laser provides pump light in the 970 nm absorption band of Yb. At the fiber output, Yb^{3+}:SiO_2 laser emission at 1042 nm and unabsorbed pump light at 972 nm are separated by a fiber-coupled WDM filter with 45 dB isolation. The coupling and laser output are monitored with an optical detector, power meter, and spectrum analyzer (0.07 nm resolution). The intrinsic microcavity quality factor is calculated by measuring the resonance linewidth in the undercoupled regime. At the pump wavelength of 972 nm, the Q is 1×10^6 due to resonant absorption by the ytterbium ions. The cavity Q at 1550 nm, well removed from the Yb absorption band, is 25×10^6 and reflects the low scattering loss of the cavity.

3.6.2 Ytterbium concentration

Since the average pump photon makes 1,000 round trips in the cavity, this Yb-doped glass laser achieves efficient pump absorption even though the Yb concentration is just 0.01%. High pump

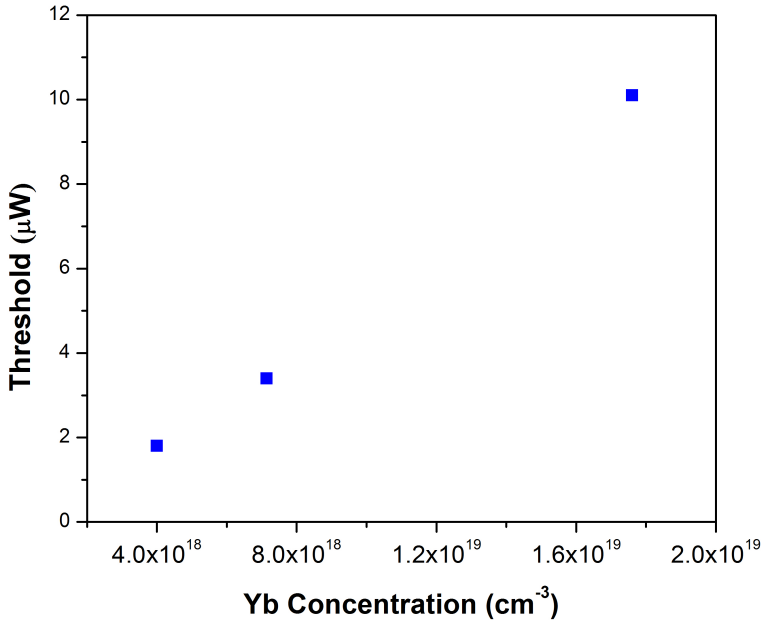

Figure 3.7. Measured laser threshold (absorbed power) as a function of Yb^{3+} concentration for Yb-doped silica microcavity

absorption, short cavity length, and low doping concentration are necessary for low lasing threshold [21]. The doping concentration must be high enough to provide sufficient gain to overcome material and cavity losses. As such, no lasing was observed for Yb concentrations as low as 1×10^8 cm^{-3} given the available pump power. But for concentrations greater than at least 4×10^8 cm^{-3}, the pump threshold was measured to increase with concentration as shown in Figure 3.7. The additional pump power is needed to compensate for the loss from unpumped Yb^{3+} ions because the ground state of Yb is well populated at room temperature.

3.6.3 Laser results

A record low 1.8 μW threshold of absorbed power was demonstrated for a 40 μm diameter silica microtoroid laser with 4×10^8 cm^{-3} Yb^{3+} concentration. To the best of the author's knowledge, this is the lowest published threshold to date for any Yb-doped laser. The laser output power depends linearly on the absorbed pump power (above threshold) as shown in Figure 3.8. The coupler, filter, and taper losses are accounted for in these results. Microtoroids support both clockwise and counterclockwise modes that are coupled by surface scattering [75]. But, only the single-end laser power from the clockwise mode is measured, discarding approximately half of the laser output power. While the laser slope efficiency with respect to absorbed power for the lowest threshold laser is 3%, slope efficiencies as high as 18% were recorded, as shown in Figure 3.8. The highest output power is 12 μW.

Continuous wave (cw) multimode lasing was demonstrated over a 40 nm span for certain taper to cavity couplings conditions, due to the broad emission bandwidth of Yb. But, with proper alignment, single frequency cw laser output is attainable (see the laser spectrum shown in Figure 3.9). The microtoroid laser cavity FSR is 6 nm.

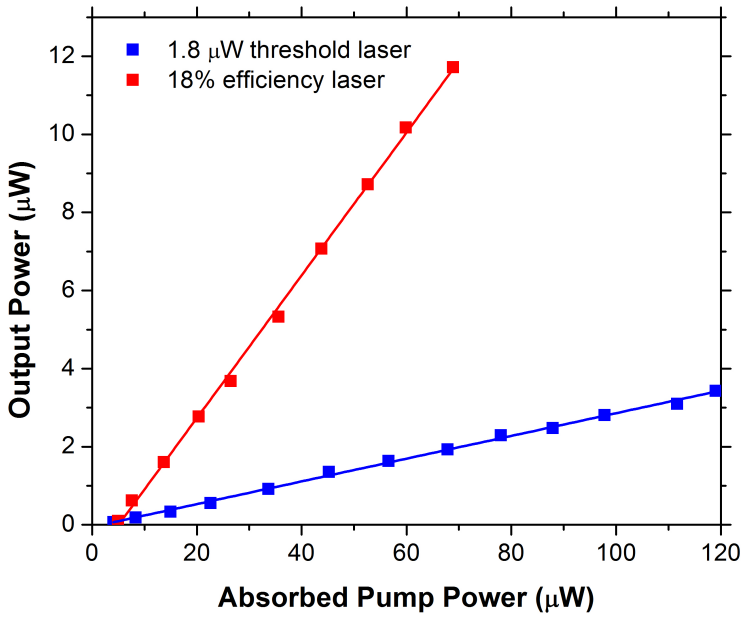

Figure 3.8. Measured laser output power as a function of absorbed pump power for two 40 μm diameter Yb^{3+}:SiO_2 microtoroid lasers. One toroid laser was overcoupled to the taper waveguide and achieved high efficiency (shown in red), the other shows low pump threshold for a slightly undercoupled taper condition (shown in blue)

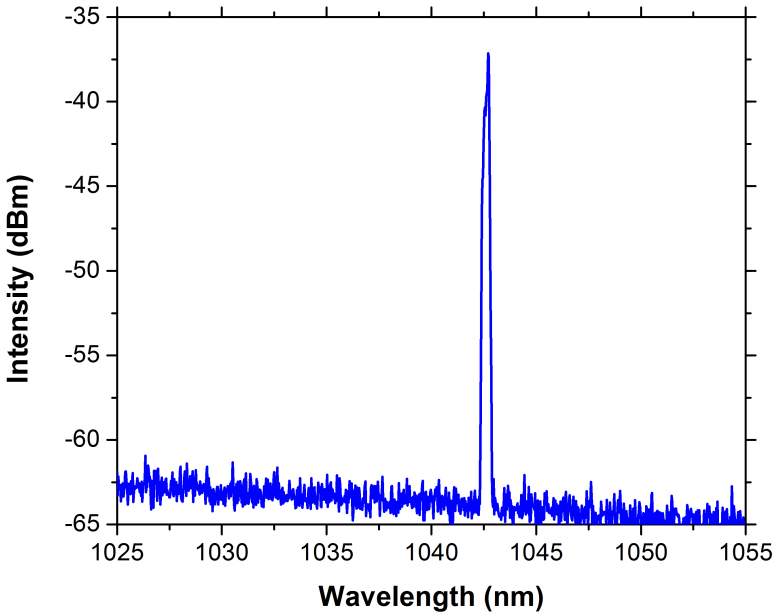

Figure 3.9. Measured laser output spectra of single-frequency Yb^{3+}:SiO_2 microtoroid laser

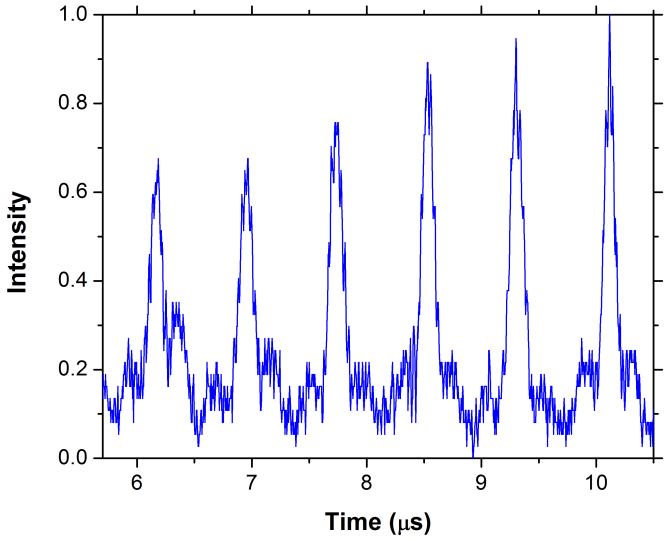

Figure 3.10. Plot of toroid laser output exhibiting 1 Mhz and 200 ns duration pulses caused by saturable absorption of unpumped Yb^{3+} ions

3.6.4 Saturable absorption induced laser pulsing

During testing, several other Yb:SiO_2 lasers exhibited pulsations in the laser output power similar to those found in an Er:SiO_2 microtoroid laser [20]. Pulsing is most easily observed for higher doping concentration (typically $2 \times 10^{19}\,\mathrm{cm}^{-3}$). Laser pulsing with 1 MHz repetition rate and 100 ns duration is presented in Figure 3.10. The origin and behavior of pulsations in Yb-doped silica microlasers is believed to be associated with saturable absorption caused by Yb ions adjacent to the laser mode that are not completed excited [62].

3.7 Summary

In conclusion, the author has demonstrated a single frequency on-chip Yb-doped silica laser fabricated by the solgel process. The pump threshold is as low as 1.8 μW, which is more than 100 times less than the lowest published threshold to date for a Yb-doped laser [54]. The slope efficiency is as high as 18%. This Yb^{3+}:SiO_2 laser will operate more efficiently in a water environment compared with a 1.55 μm laser, since the absorption coefficient of water is significantly less at 1.0 μm compared with 1.55 μm (0.16 and 12 cm^{-1}, respectively) [22]. As such, it could function as the laser for an active chemical or biological sensor using surface functionilized protocols readily available for silica. Also, the flexible solgel process and compatibility of the simple electronic structure of Yb with other rare-earth ions can be used in the future for dual-doped lasers such as Er^{3+},Yb^{3+}:SiO_2; a subnanosecond Q-switched Cr^{4+},Yb^{3+}:SiO_2 laser [76]; or upconversion lasers [77]. Applications for this low threshold and small footprint laser may be found in dense on-chip optical communications, active sensors, and rare-earth visible lasers.